Improving suspicious breast lesion characterization using semi-automatic lesion fractional volume washout kinetic analysis

Jie Huang[a)]
Department of Radiology, Michigan State University, East Lansing, Michigan 48824

Tobias Hahn
Department of Radiology, Michigan State University, East Lansing, Michigan 48824 and
Department of Physics and Astronomy, Michigan State University, East Lansing, Michigan 48824

Lori Hoisington, Sarah Schafer, Xiaopeng Zong, and Kevin Berger
Department of Radiology, Michigan State University, East Lansing, Michigan 48824

(Received 30 March 2011; revised 19 September 2011; accepted for publication 20 September 2011; published 19 October 2011)

Purpose: Although breast dynamic contrast-enhanced magnetic resonance imaging (DCE-MRI) demonstrates high sensitivity for malignant tumor detection, a major limitation is the relative low specificity, resulting in many false-positive diagnoses of suspicious lesions (BI-RADS assessment of 4 or 5) in clinical practice and consequently producing a relatively low positive predictive value (PPV) for biopsies. The most enhanced areas in the malignant tumors show a typical washout (WO) kinetic feature for the postcontrast signal intensity time courses and also correlate with microvessel density. Benign proliferative breast diseases can also produce the WO curve, yielding an equivocal kinetic behavior for the benign lesions and rendering their diagnoses as suspicious lesions in clinical practice. Considering that tumor angiogenesis is essential to an aggressive cancer tumor growth, the authors hypothesize that the WO volume fraction, i.e., the total volume of the WO voxels that demonstrate the WO curve within the tumor, is relatively large for malignant tumors in comparison to that for benign lesions. In this study, the authors present a lesion fractional volume WO kinetic analysis for improving the characterization of suspicious breast lesions.
Methods: A method to automatically detect the boundary of a manually selected contrast-enhanced lesion was introduced and tested, utilizing the signal intensity difference between the contrast-enhanced lesion and its surrounding tissues. The kinetic features of the postcontrast signal intensity time courses were quantitatively analyzed voxel-by-voxel with emphasis on the examination of the WO behavior. The WO volume fraction relative to the whole lesion volume was introduced and tested as a biomarker for improving the characterization of suspicious breast lesions. The sample for this test consisted of 28 suspicious lesions with correlative histopathology reports available. The lesions included 10 malignant tumors and 18 benign lesions, yielding a 35.7% PPV of the biopsies.
Results: The semi-automatic method produced an objective volume of interest for each lesion with voxelwise-quantified kinetic features. With an optimal choice of kinetic analysis, the mean and standard deviation of the WO volume fraction were 59.1 ± 13.1 (%) with the range from 41.0% to 80.7% for the malignant tumors and 31.4 ± 20.5 (%) with the range between 3.3% and 71.6% for the benign lesions, respectively. The WO volume fraction was significantly larger ($p < 0.0004$) for the malignant tumors than for the benign lesions. While maintaining the same sensitivity for malignant tumors, using the WO volume fraction as an additional biomarker would characterize 14 out of the 18 benign lesions as benign, potentially resulting in an 100% improvement rate in the PPV of the biopsies (from 35.7% to 71.4%) and consequently a 77.8% reduction rate in potentially unnecessary biopsies (from 18 to 4).
Conclusions: The significantly larger WO volume fraction for the malignant tumors was probably related to the increased vascularity associated with tumor angiogenesis. The results suggest that the WO volume fraction biomarker has potential to improve the computer-based assessment of breast MRI by greatly increasing the PPV of breast biopsies and potentially significantly reducing the number of unnecessary biopsies without compromising sensitivity. © *2011 American Association of Physicists in Medicine*. [DOI: 10.1118/1.3651635]

Key words: breast MRI, DCE-MRI, breast tumor characterization, washout curve, WO volume fraction

I. INTRODUCTION

Breast magnetic resonance imaging (MRI) has evolved into a useful clinical tool for breast tumor detection and local staging of cancer, and breast dynamic contrast-enhanced (DCE) MRI has been shown to be very sensitive for malignant tumor (MT) detection.[1–10] Early studies of contrast-enhanced breast MRI demonstrated early enhancement of malignant tumors following an intravenous injection of

gadolinium diethylenetriamine-pentaacetic acid (Gd-DTPA).[1,2] Further investigation, however, revealed that many benign lesions (BLs) also demonstrate the same initial enhancement as malignant tumors.[3,4] Malignant tumors often demonstrate a rapid increase in signal intensity after contrast administration and then reach a peak around 1–3 min followed by a washout (WO) or plateau (PL) behavior on delayed phase images. In contrast, benign lesions often exhibit a slower but persistent enhancement (PE) without the WO behavior.[6] The early enhancement in malignant tumors is probably related to tumor angiogenesis.[11–14]

Although DCE-MRI demonstrates high sensitivity for malignant breast tumor detection, a major limitation is the relative low specificity. Suspicious enhancement curves are frequently observed in many benign lesions including fibroadenomas, proliferative fibrocystic changes, atypical ductal hyperplasia, etc.,[3,4,15,16] indicating the limitation of enhancement analysis in the differentiation of benign versus malignant lesions. This phenomenon leads to many false-positive diagnoses of suspicious breast lesions in clinical practice and produces a relatively low positive predictive value (PPV) for biopsies (the number of cancers detected divided by the number of biopsies performed).[3,4,6,7] In a recent study involving a total of 125 breast lesions that were either categorized as suspicious abnormality (BI-RADS assessment of 4) or highly suggestive of malignancy (BI-RADS assessment of 5), the breast biopsies resulted in 42 malignant tumors and 83 benign lesions, showing a 33.6% PPV of the biopsies and consequently a 66.4% false-positive rate of benign biopsies (the ratio of biopsied benign lesions to the number of biopsies performed) at the clinic.[17]

Previous research shows that kinetic features of the postcontrast signal intensity time courses correlate with microvessel density; the WO curve has the highest microvessel density followed by the PL curve and then the PE curve with the lowest microvessel density.[12] Malignant tumors have a higher rate of small vessel angiogenesis compared to benign lesions. One study demonstrated that the most enhanced areas in malignant tumors showed a typical WO curve and also correlated with microvessel density.[14] These findings imply that the WO curve may reflect the hypervascularity associated with tumor angiogenesis in a malignant tumor. They further suggest that the total volume of the WO voxels that demonstrate the WO curve within the tumor may provide a measure to quantify the hypervascularity of the tumor. Accordingly, the WO volume fraction characterized as the ratio of the total volume of the WO voxels to the whole tumor volume has the potential to be a biomarker for quantifying the hypervascularity associated with tumor angiogenesis. While benign proliferative breast diseases can also produce the WO curve, yielding an equivocal kinetic behavior between benign and malignant lesions and making them difficult to distinguish, the WO volume fraction for benign proliferation should be relatively small in comparison to that for tumor angiogenesis in malignant tumors, considering that tumor angiogenesis is essential to an aggressive cancer tumor growth. Thus, measuring the WO volume fraction may help to differentiate benign from malignant contrast-enhancing lesions.

In current standard ACR BI-RADS MR imaging lexicon, the WO curve is only qualitatively but not quantitatively defined. It is a washout curve when there has been a decrease in signal intensity after peak enhancement has been reached within 1 to 3 min.[18] Computing WO volume fraction requires (1) determining the boundary of a lesion, (2) quantifying the postcontrast kinetic curve for each voxel within the lesion, (3) defining WO voxels, and then (4) computing the WO volume fraction relative to the whole lesion volume.

In this study in order to objectively measure the WO volume fraction, we first introduce a method to automatically determine the boundary of a manually selected DCE lesion. A linear fitting of the postcontrast signal intensity time course is performed and then the slope of the fitted line is computed voxel-by-voxel; a negative slope indicates a WO curve, a zero slope a PL curve, and a positive slope a PE curve. The study consists of two parts. Study I tests the feasibility of the introduced approach for calculating lesion WO volume fraction and using this measure to differentiate benign from malignant lesions for a selected lesion set. Study II examines the potential effectiveness of using WO volume fraction to improve the characterization of suspicious breast lesions from our clinical breast DCE-MRI data.

II. MATERIALS AND METHODS

II.A. Lesion selection

Patients who underwent standard clinical breast MRI examination at Michigan State University (MSU) Radiology between January of 2007 and September of 2009 were retrospectively reviewed for abnormal contrast-enhancing breast lesions. For study I, a total of 16 biopsy-proven lesions involving 15 women (ages from 33 to 61 with mean $\pm$ SD $=$ 49.6 $\pm$ 8.3 yr) were selected for testing the feasibility of the proposed approach for calculating lesion WO volume fraction and using this measure to differentiate benignity from malignancy for the selected lesions. Among these lesions, 11 were malignant tumors (infiltrating invasive ductal carcinoma) and the remaining 5 were benign lesions (fibrocystic disease or fibroadenoma). Study II included mass-like enhancing lesions that were larger than 5 mm. These lesions were initially detected on breast MRI and were assigned a BI-RADS assessment of 4 or 5. This resulted in a total of 43 suspicious lesions from a total of over 650 clinical breast MRI examinations. Lesions with BI-RADS assessment of 6 (known biopsy-proven malignancy) were not included in this study. We also excluded those lesions with BI-RADS assessment of 4 or 5 that did not undergo biopsy or did not include histopathology reports (15 lesions in total out of the 43 suspicious lesions). As a result, a total of 28 suspicious contrast-enhanced lesions (25 lesions with BI-RADS assessment of 4 and 3 lesions with BI-RADS assessment of 5) in 27 patients (53.8 $\pm$ 12.9 yr, ranged from 33 to 81 yr) had subsequent biopsy with available histopathology reports and comprised the lesion set for study II. The biopsies resulted in 10 malignant tumors (the 3 highly suggestive of malignant lesions with BI-RADS assessment of 5 plus 7 lesions with BI-RADS assessment of 4) and 18 benign lesions. This yielded a 35.7% PPV of the biopsies and consequently a 64.3% rate for

potentially unnecessary biopsies. The malignant tumors include seven infiltrating ductal carcinoma and/or DCIS and three invasive lobular carcinomas. The benign lesions include fibrocystic changes, fibrosis, and fibroadenoma. All of the lesions included were radiologically diagnosed by board-certified, experienced diagnostic radiologists in the Department of Radiology at MSU, and these diagnoses were reached clinically, independent of this study. The diagnoses followed the current standard ACR BI-RADS MR imaging lexicon, including the evaluation of lesion morphology and kinetic enhancement analysis using CADSTREAM software (Merge CAD, version 4.1.0). This study was approved by the University Institutional Review Board at MSU.

II.B. MRI acquisition

Bilateral breast imaging was performed on a 1.5 T clinical scanner (General Electric HealthCare, Milwaukee, WI) using a dedicated bilateral 8-channel breast array coil (ASSET: slice acceleration factor 1.0 and phase acceleration factor 3.0). An intravenous line was established before imaging for later delivery of gadobenate dimeglumine (Gd-BOPTA) contrast agent (0.1 mmol/kg), and the contrast agent was injected at a rate of 3 cc/s followed by a 20-cc saline solution flush administered at the same rate. The total amount of administered contrast agent to a patient depended on the patient's body weight, and the maximum amount of administered contrast agent to any patient is limited to 20 cc. One set of precontrast images was acquired immediately prior to the administration of the contrast agent. The contrast agent injection and the MR dynamic imaging acquisition were synchronized, and the first postcontrast phase was initiated after a 30 s scan delay. Postcontrast imaging included five dynamic phases with a scan time of 90 s for each phase. The total scan time for postcontrast imaging was 7.5 min. Dynamic images were acquired in the axial plane using a 3D, fat-suppressed T1-weighted fast spoiled-gradient-echo pulse sequence with the following parameters: TE/TR = 2.8/5.9 ms, field of view 320 mm, matrix 320×320, flip angle 10°, slice thickness 2 mm, 116 locations per slab, number of excitations (NEX) 0.76, and ZIP2. The fractional NEX 0.76 was applied in the phase direction for shortening the acquisition time (only 76% of the 320 phase steps in k-space were applied), and images were reconstructed to an in-plane resolution of 512×512 pixels. ZIP2 is a zero fill interpolation processing technique that improves through-plane resolution by a factor of 2 via interpolating the acquired images to create new images, and the application of ZIP2 resulted in the reconstructed dynamic images with a voxel resolution of $0.625 \times 0.625 \times 1$ mm^3. A representative contrast-enhanced lesion for the precontrast and postcontrast five dynamic phases is shown on the top panel in Fig. 1.

II.C. Motion correction

Possible motion artifacts due to breathing or unexpected body movements were examined between the different phases via comparing the shape of apparent breast landmarks such as nipples. Any shift perpendicular to the image plane was examined first, and we did not notice any substantial shift larger than one slice in our data. Accordingly, no motion correction was conducted in this direction. We then examined any in-plane shift in other phases relative to the first postcontrast phase. Small shifts in both directions were noticed and subsequently corrected. A MATLAB-based software program was implemented to correct these in-plane motion artifacts by shifting the examined image in both directions until a best possible overlap of the landmarks (such as the nipple or breast edge) was found between the examined image and the reference image. The effect of this motion correction on the computed WO volume fraction was assessed with one lesion; the difference in the WO volume fraction was found to be less than 1% with and without the motion correction, indicating that the computed WO volume fraction was not sensitive to the motion correction. The group-averaged in-plane mean shift was 0.55 voxels (0.34 mm) in the anterior/posterior direction and 0.25 voxels (0.16 mm) in the left/right direction. Among all images, the maximum shift of three voxels (1.88 mm) was found in the anterior/posterior direction and two voxels (1.25 mm) in the left/right direction.

II.D. Lesion boundary determination

A MATLAB-based software algorithm for determining lesion boundary was developed and tested in study I. The contrast-enhanced lesions on the first postcontrast images (phase 1, t = 1.5 min) were identified and confirmed by a board-certified radiologist. For each lesion, the boundary of the lesion on each slice was automatically determined using the in-house developed algorithm. First, an inner-boundary within the lesion and an outer-boundary outside of the lesion were manually drawn, and then, a region of interest (ROI) was drawn to roughly circumscribe the lesion. Second, the software computed the mean (μ) and standard deviation (σ) of the signal intensity of the voxels within the ROI. A threshold $TH = \mu - 1.75\sigma$ (one-tail probability <4%) was computed, and then used to examine the voxels between the inner- and outer-boundaries. If a voxel's signal intensity was larger than TH, the voxel was included into the ROI. If the signal intensity was smaller than TH, the voxel was removed from the ROI. This resulted in a new ROI. (The new ROI was limited to the area between the predetermined inner- and outer-boundaries.) Then, the software computed μ and σ for the new ROI and iterated the process automatically until a stable ROI was reached. Finally, this stable ROI was used to represent the lesion. After having found the lesion area, a layer of one voxel width was generated as a gap between the lesion and the bordering tissue, as illustrated in Fig. 1, bottom panel (A). The same total area size as the lesion area size was generated in the bordering tissue to represent an ROI for the bordering tissue. The lesion ROI and the bordering tissue ROI were separated by the gap represented by the inner ring in Fig. 1, bottom panel (A). A second adjacent tissue ROI with the same total area size was also generated outside the bordering tissue ROI as shown in Fig. 1, bottom panel (A). These generated ROIs also served as lesion masks for the precontrast images and the other four phases of

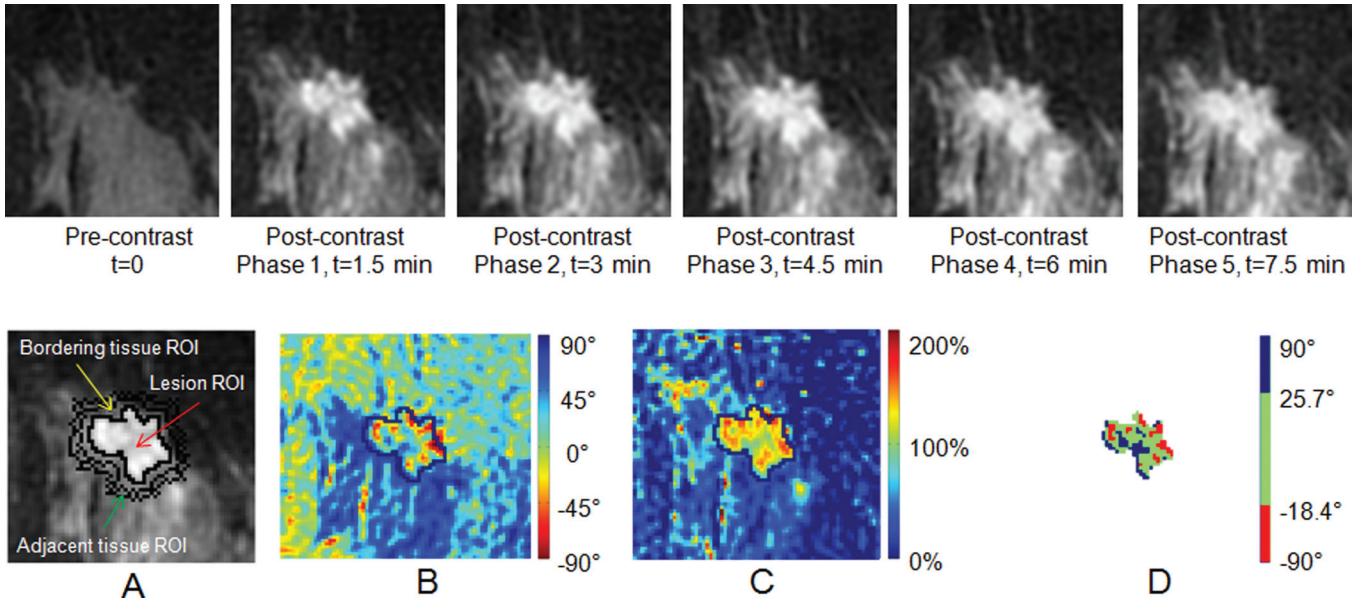

FIG. 1. Top panel: A representative contrast-enhanced lesion for the precontrast and postcontrast five dynamic phases. Bottom panel: (A) Illustration of a lesion ROI, a bordering tissue ROI, and an adjacent tissue ROI, respectively, based on the first postcontrast image (phase 1, t = 1.5 min). The inner black ring denotes one voxel gap between the lesion and the bordering tissue; the middle black ring denotes the last voxel layer of the bordering tissue ROI, and likewise the outer black ring denotes the last voxel layer of the adjacent tissue ROI. All three ROIs have the same total area size (same voxel numbers within each ROI). (B) Corresponding image of the angle of the slope of the fitted straight lines for the postcontrast period (details see Fig. 2). (C) Distribution of relative uptake (wash-in) signal intensity change between the first postcontrast image and the precontrast image. (D) Illustration of cluster distribution for the three kinetic features of WO (red, $-90° < \alpha < -18.4°$), PL (green, $-18.4° \leq \alpha \leq 25.7°$), and PE (blue, $25.7° < \alpha < 90°$).

postcontrast images. The signal intensities of the three ROIs were computed for testing the reliability of lesion boundary detection.

Breast tumors are often heterogeneous in enhancement because some areas such as those that result from tumor necrosis may not enhance. If these nonenhancing areas in the lesion ROI were included in subsequent computations, then the resulting WO volume fraction could potentially be incorrect and unreliable, particularly for large necrotic tumors. To prevent this potential error, the final TH value of the final stable lesion ROI was utilized to detect and exclude these nonenhancing areas. Voxels within the final stable lesion ROI were excluded if their signal intensities were smaller than the TH value, forming a lesion ROI mask which was used for the subsequent computations.

II.E. Quantitative kinetic feature analysis

We introduced and tested a method to depict the overall postcontrast kinetic curve in study I. To quantitatively examine the overall postcontrast kinetic feature of a voxel, the signal intensity time course of the five dynamic postcontrast phases of the voxel was linearly fitted using the method of least-squares, and then the slope (m) of the fitted straight line was further computed. A negative slope characterizes a WO curve and a positive slope characterizes a PE curve (Fig. 2). To maximize the variation in the slope of MR signal versus time for both lesion and surrounding tissue ROIs of all lesions, the time axis was rescaled to 80 units between each consecutive phase (corresponding 1.125 s per unit). Letting α be the angle between the fitted straight line and the horizontal axis, its relation with the slope m is determined by the equation $m = \tan(\alpha)$. Thus, the corresponding angle of the fitted straight line was computed using $\alpha = \arctan(m) \times 180/\pi$, providing a means of characterizing the kinetic features voxel-by-voxel as illustrated in Fig. 1, bottom panel (B). (Note that this computed angle is in the range between $-90°$ and $90°$.) Accordingly, a negative angle characterizes a WO curve and a positive angle characterizes a PE curve (Fig. 2). A histogram of the slope angle distribution was further computed for each lesion, summing voxel values for all slices covering the lesion, and then a final group histogram was computed for the malignant tumors and the benign lesions, respectively (Fig. 3). As shown in Fig. 3(A), the group histogram for the malignant tumors showed an approximate Gaussian distribution with $\mu = 3.65°$ and $\sigma = 32.39°$. This approximate Gaussian distribution enabled us to establish a kinetic feature-based statistical model. The center part of the distribution (around $0°$) characterizes the well-recognized PL behavior (type II), the left end of the distribution (negative angle) characterizes the WO behavior (type III), and the right end (positive angle) reflects the PE behavior (type I).[6]

II.F. Lesion WO volume fraction test

The descriptions of the three kinetic features are only qualitative but not quantitative, i.e., there is no clear cutoff boundary between WO and PL behaviors as well as between PL and PE behaviors. In other word, these two cutoff boundaries can be arbitrarily defined. The established kinetic feature-based statistical model in Fig. 3(A) enables us to test (1) different choices of cutoff slope angle for defining WO curves and (2) the effects of these choices on the differentiation of the benign lesions from the malignant tumors in study

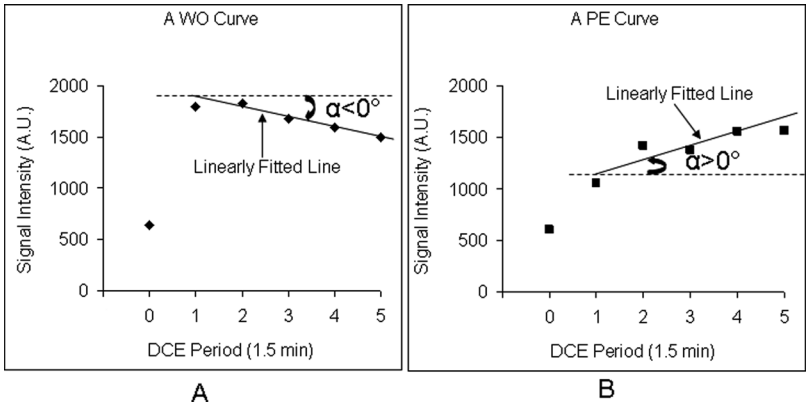

FIG. 2. Illustration of linear fitting the signal intensity time course of the postcontrast five phases (1, 2, 3, 4, 5) using the least-squares method. The angle (α) between the fitted straight line and the horizontal line was computed using $\alpha = \text{atan}(m) \times 180/\pi$, where m is the slope of the fitted straight line. A: a negative α characterizes a WO curve; B: a positive α characterizes a PE curve. A.U.: arbitrary unit.

I. We selected three different choices for testing(1) a 25% volume fraction for the WO curves ($-90° < \alpha < -18.4°$), a 50% volume fraction for the PL curves ($-18.4° \leq \alpha \leq 25.7°$), and the remaining 25% volume fraction for the PE curves ($25.7° < \alpha < 90°$) [Fig. 3(A)]; (2) a 16% volume fraction for the WO curves ($-90° < \alpha < -28.6°$), a 68% volume fraction for the PL curves ($-28.6° \leq \alpha \leq 35.9°$), and the remaining 16% volume fraction for the PE curves ($35.9° < \alpha < 90°$); and (3) a 45.6% volume fraction for the WO curves ($\alpha < 0°$) and the remaining 54.4% volume fraction for both PL and PE curves ($\alpha \geq 0°$). (These selected volume fraction values represent the corresponding areas under the Gaussian distribution curve in Fig. 3(A) for the three corresponding kinetic curves for the three selected choices, respectively.) A WO voxel was defined as a voxel showing a WO curve, a PL voxel as a voxel showing a PL curve, and a PE voxel showing a PE curve. The WO volume fraction for a lesion was computed as the ratio of the sum of all WO voxels within the lesion to the lesion volume computed as the sum of all enhancing voxels within the lesion. The PL and PE volume fractions for the lesion were also computed in the same way. The computed volume fraction values for the selected lesions in study I were compared with their corresponding statistical model values to test (1) whether the WO volume fraction can be used as a biomarker for differentiating the benign lesions from the malignant tumors and (2) whether these three cutoff boundary choices have any significant effect on the differentiation of the benign lesions from the malignant tumors.

II.G. Test for improving the characterization of suspicious breast lesions

In study I, we tested the feasibility of using WO volume fraction to differentiate benignity from malignancy for the selected lesions. The study showed that the WO volume fraction was effective for the differentiation, and all three selected choices for cutoff boundaries produced similar results. Considering that, for a given signal intensity time course, the computed slope value depends on the choice of the time unit for the postcontrast five dynamic phases. Consequently, the WO volume fraction values for both cutoff boundary choices (1) and (2) vary with the choice of the time unit. In practical application, it is desirable for the computed WO volume fraction to be independent of the choice of the time unit. Since the computed WO volume fraction value for the cutoff boundary choice (3) remains unchanged for different choices of the time unit, for further testing we selected choice (3) for defining WO curves, i.e., a WO curve was defined as $\alpha < 0°$.

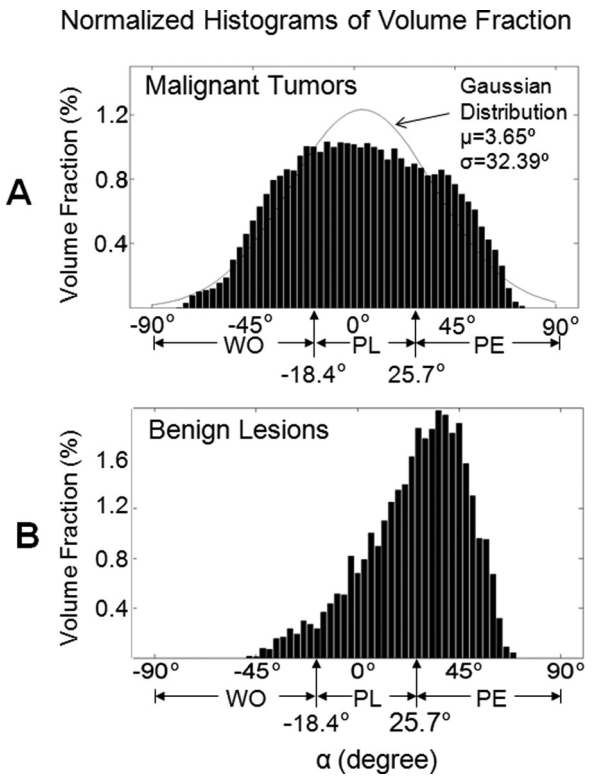

FIG. 3. Normalized histograms of volume fraction versus the angle α of the slope of the fitted straight lines for the selected lesions in study I. (A) The normalized histogram of the eleven malignant tumors. The magnitude of bars represent volume fraction relative to the total volume of all eleven malignant tumors, and the bar width is 3°. The solid curve represents the Gaussian distribution with $\mu = 3.65°$ and $\sigma = 32.39°$, and the total area under the curve equals 100% volume fraction. The vertical arrow-line labeled as $-18.4°$ represents the cutoff angle for separating WO curves from PL curves, and the vertical arrow-line labeled as 25.7° represents the cutoff angle between PL curves and PE curves, i.e., the cutoff boundary choice (1) in Sec. II F. Lesion WO volume fraction test. (B) The normalized histogram of the five benign lesions.

We tested whether the WO volume fraction can improve the characterization of the suspicious breast lesions in study II. An all new set of 28 suspicious breast lesions in study II were identified by a board-certified, experienced breast MRI diagnostic radiologist. To begin, the radiologist identified the start and end slices of a lesion on the first phase, postcontrast images. Then, using the previously validated software algorithm, a trained research assistant completed the determination of the lesion boundary on each slice from the start to end slices of the lesion. The radiologist confirmed the determined lesion boundary on each slice and did not need to modify the automatically determined lesion boundary on any slice for any of the 28 lesions. Another experienced breast MRI diagnostic radiologist also independently examined the determined lesion ROIs on each slice for each lesion. This radiologist did not make any change on the determined lesion ROIs for 23 lesions out of the 28 lesions. For the other five lesions including two MTs and three BLs, the lesion volume and WO volume fraction changes were (1) 2.09 → 2.11 (cm^3) and 26.5% → 26.3% (MT1), (2) 0.57 → 0.65 (cm^3) and 50.1% → 49.9% (MT2), (3) 0.74 → 0.48 (cm^3) and 2.2% → 1.5% (BL1), (4) 0.84 → 0.18 (cm^3) and 6.8% → 4.3% (BL2), and (5) 6.29 → 0.29 (cm^3) and 17.8% → 23.5% (BL3). Overall there were significant changes to lesion volumes in two cases largely secondary to reader subjective interpretation of mass-like enhancement versus regional or ductal enhancement pattern. Regardless, the WO volume fraction changes averaged 0.33% for the 28 lesions, demonstrating the relative reader-independent reproducability of the technique. Figure 4 illustrates a lesion ROI on each slice in comparison to the precontrast and first postcontrast images, respectively. The sum of areas of the lesion ROI over the slices that cover the whole lesion yielded the volume of interest of the lesion. After that, the quantitative kinetic feature analysis and the WO volume fraction computation of the lesion were automatically completed by the software. The lesion boundary determinations and the WO volume fraction computations were blinded to the histopathology reports.

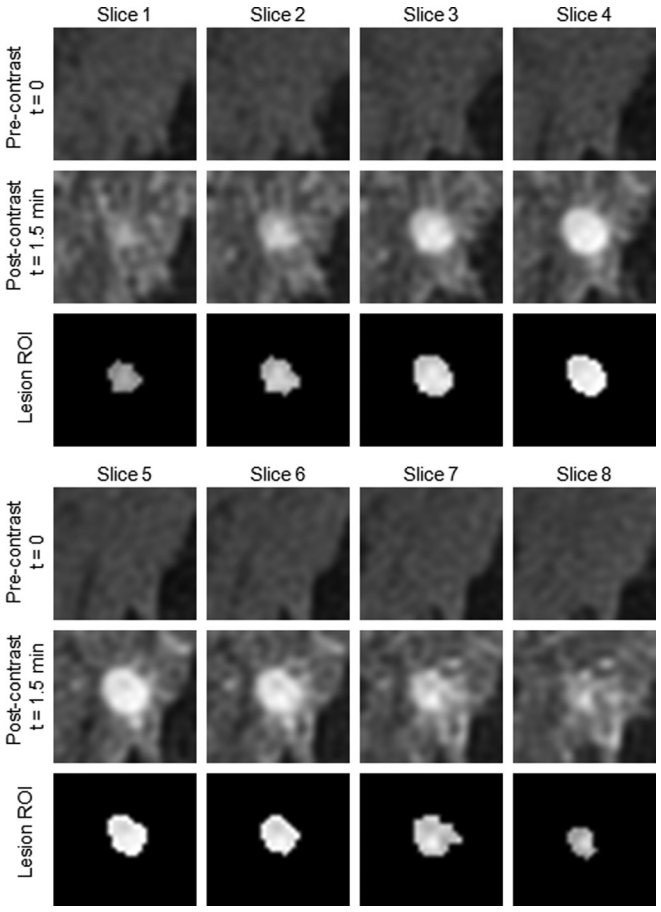

FIG. 4. Illustration of a lesion ROI on each slice in comparison to the precontrast and first postcontrast images, respectively. The lesion was not apparent on the precontrast images but was visible on the first postcontrast images due to the lesion's increased contrast-enhancement relative to its bordering tissue. The lesion boundary was determined based on this difference in contrast-enhancement between the lesion and its bordering tissue. For details, see Sec. II D. Lesion boundary determination.

III. RESULTS

III.A. Lesion boundary determination

In study I, we first tested the reproducibility of our method to automatically determine the lesion boundary with five threshold values (TH = $\mu - 1.25\sigma$, $\mu - 1.5\sigma$, $\mu - 1.75\sigma$, $\mu - 2.0\sigma$, and $\mu - 2.25\sigma$). We found that all three median threshold values produced a reasonable lesion ROI, which separated the contrast-enhanced lesion from the much less enhanced surrounding tissues. Based on theoretical considerations, it is desirable that the technique produces a final lesion ROI that is not sensitive to the initially drawn ROI that roughly circumscribed the lesion. For this purpose, we further tested the reproducibility of the determined lesion ROI by varying the shape of the initially drawn ROI. We found that the threshold TH = $\mu - 1.75\sigma$ produced a lesion boundary that was very well reproducible and virtually independent of the initially drawn ROI shape, resulting in an objective lesion ROI. This final lesion ROI was confirmed to be reliable for representing the lesion by a board-certified experienced diagnostic radiologist. For the threshold TH = $\mu - 1.75\sigma$, our method in more than 180 tests always produced a satisfactory lesion ROI.

To test the reliability of our method for lesion determination, we compared the signal intensity of the lesion ROI with that of the surrounding tissues using the first postcontrast images. The signal intensity was 1582 ± 334 ($\mu \pm \sigma$) for the lesions, 673 ± 161 for the bordering tissue ROI, and 583 ± 142 for the adjacent tissue ROI. The signal intensity of the lesions was significantly larger than that of the surrounding tissues (t-test, $p < 10^{-7}$), but, as expected, no significant difference was observed between the bordering tissue ROI and the adjacent tissue ROI ($p > 0.10$). These results indicated the reliability of our method for determining the lesion boundary. This method objectively defined contrast-enhanced lesions from surrounding tissues.

To further test the reliability of our method for lesion determination, we computed the relative uptake signal change (wash-in rate) between the first postcontrast image (I_1) and the precontrast image (I_0), i.e., $(I_1 - I_0)/I_0$,

[Fig. 1, bottom panel (C)]. The wash-in rate was 111 ± 39 (%) for the benign lesions and 50 ± 20 (%) for their bordering tissues, and the difference was significant ($p < 0.009$) (Fig. 5). These results further demonstrated the reliability of the lesion determination. Similarly, the wash-in rate was 140 ± 33 (%) for the malignant tumors and 62 ± 27 (%) for their bordering tissues, and the difference was also significant ($p < 10^{-4}$). However, no significant difference was observed between the benign lesions and the malignant tumors ($p > 0.16$), consistent with their similar radiologic reports of suspicious for malignancy. We also compared the kinetic behaviors of the ROI-averaged signal intensity time courses for the malignant tumor ROI, the benign lesion ROI, the bordering tissue ROI, and the adjacent tissue ROI (data not shown). As expected, the comparison showed a dramatic difference in kinetic behavior between the lesions and the surrounding tissues but a similar kinetic behavior between the benign lesions and the malignant tumors as well as between the bordering tissue and the adjacent tissue.

III.B. Lesion WO volume fraction test

To better understand the underlying cause of the difficulty in the differentiation of the false positives (the benign lesions) from the true positives (the malignant tumors), we first plotted the mean kinetic curves for WO, PL, and PE for the cutoff boundary choice (1), (Fig. 6). As can be seen, all three kinetic curves showed similar features between the malignant tumors and the benign lesions. For both the malignant tumors and the benign lesions, the WO cluster had the largest uptake signal intensity change followed by the PL cluster and then the PE cluster. The WO cluster represented the most enhanced area within the lesion and showed the typical type III behavior for both the malignant tumors and the benign lesions [Fig. 1, bottom panel (C) and (D)]. Accordingly, if the most enhanced area is selected as an ROI for the lesion diagnosis as recommended by the current standard ACR BI-RADS MR imaging lexicon, the typical type III behavior of thus selected ROI for the benign lesions should characterize them as suspicious for malignancy as confirmed with their radiologic reports, rendering the diagnosis as a false positive error. It is mainly the coexistence of WO behavior within the benign lesions that leads to the false positive diagnoses.

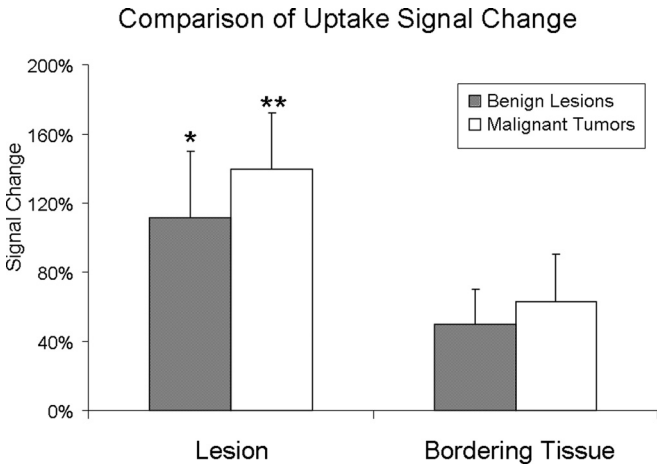

FIG. 5. Relative uptake signal changes (wash-in rate) between the first postcontrast image and the precontrast image for the selected lesions in study I. The wash-in rate was significantly larger for both the benign lesions (*$p < 0.009$) and the malignant tumors (**$p < 10^{-4}$) in comparison to the bordering tissue ROI. No significant difference between the benign lesions and the malignant tumors ($p > 0.16$). The error bar denotes σ.

Although the benign lesions and the malignant tumors showed a similar wash-in rate with similar kinetic features, the relative number of WO voxels was subsequently different between them as depicted in the histograms in Fig. 3. For the cutoff boundary choice (1), the mean volume fraction of the malignant tumors was 28.3 ± 19.8 (%) for WO, 44.3 ± 15.2 (%) for PL, and 27.4 ± 12.0 (%) for PE (Fig. 7). These values agree with the statistical model-predicted values: 25%, 50%, and 25%, respectively. For the benign lesions, however, the volume fraction was 1.7 ± 1.1 (%) for WO, 28.7 ± 11.9 (%) for PL, and 69.6 ± 12.8 (%) for PE. The PL volume fraction of the benign lesions was marginally smaller than that of the malignant tumors ($p < 0.051$). The WO volume fraction of the benign lesions was significantly smaller than that of the malignant tumors ($p < 0.002$), but the PE volume fraction of the former was significantly larger than that of the latter ($p < 0.0004$), reflecting the differences in the histograms (Fig. 3). In short, the significant difference in WO volume fraction between the benign lesions and the malignant tumors provides an additional measure for potentially improving the differentiation of benignity from malignancy of contrast-enhancing breast lesions. For the cutoff boundary choice (2), the mean WO volume fraction was 19.1 ± 16.0 (%) for the malignant tumors and 0.7 ± 0.6 (%) for the benign lesions, and these values are also significantly different from one another ($p < 0.004$). Similarly, for the cutoff boundary choice (3), the mean WO volume fraction of $45.8.1 \pm 19.7$ (%) for the malignant tumors was found again to be significantly different from that of 8.4 ± 5.7 (%) for the benign lesions ($p < 0.001$). These results demonstrate that, although the WO volume fraction value varied from choice-to-choice, the introduced technique of using the WO volume fraction as a biomarker for differentiating the benign lesions from the malignant tumors does not depend on these statistical modeling choices (Fig. 8).

III.C. Test for improving the characterization of suspicious breast lesions

In study II, we examined the effectiveness of using WO volume fraction to improve the characterization of the 28 suspicious breast lesions from our clinical breast DCE-MRI data (10 malignant tumors and 18 benign lesions). The cutoff boundary choice (3) was used in this test. For the 10 malignant tumors, the mean and standard deviation of the WO volume fraction was 45.3 ± 14.6 (%) with the range from 26.5% to 68.1%. (This mean value of 45.3% agrees very well with the mean value of 45.8% for the 11 infiltrating ductal carcinoma tumors in study I.) For the 18 benign lesions, however, the mean and standard deviation of the WO volume fraction was 21.8 ± 19.0 (%) with the range

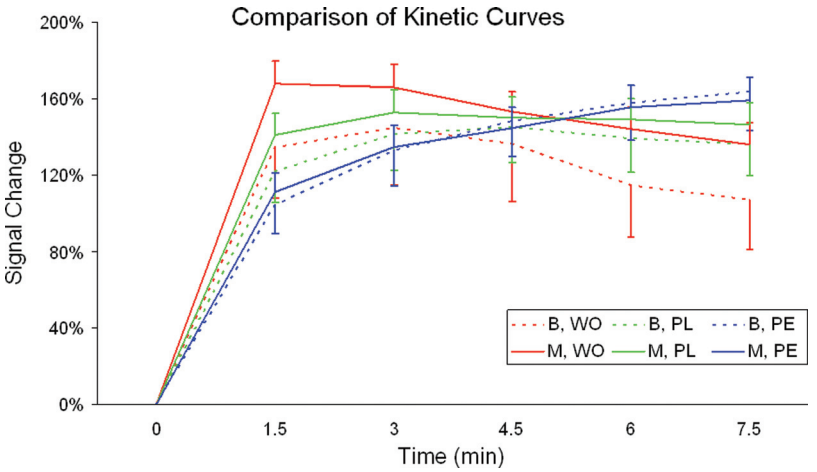

FIG. 6. The mean kinetic curves of WO, PL, and PE clusters [Fig. 1(D)] for the selected lesions in study I. The plotted signal change represents the postcontrast signal intensity change at each time point relative to the precontrast signal intensity. B, benign lesions (dashed-lines); M, malignant tumors (solid-lines). The coexistence of WO behavior (red dashed-line) in the benign lesions makes it hard to distinguish between the benign lesions and the malignant tumors (red solid-line). The error bar denotes SEM.

between 2.2% and 64.7%, significantly smaller than the value for the malignant tumors ($p < 0.001$). Figure 9(A) shows a scatter plot of WO volume fraction versus lesion volume for the 28 suspicious breast lesions.

Considering that the peak uptake time-point may occur after the first postcontrast phase and if so including this time-point into the linear fitting would yield a bias to the fitted line, we examined the effects of the least-squares linear fitting of the postcontrast signal intensity time course using (1) the last four dynamic phases and (2) the last three dynamic phases. Using the last four phases, the mean and standard deviation of the WO volume fraction was 59.1 ± 13.1 (%) with the range from 41.0% to 80.7% for the 10 malignant tumors. The mean and standard deviation of the WO volume fraction was 31.4 ± 20.5 (%) with the range from 3.3% to 71.6% for the 18 benign lesions, significantly smaller than the value for the malignant tumors ($p < 0.0004$). Using the last three phases, the mean and standard deviation of the WO volume fraction was 59.2 ± 14.7 (%) with the range from 38.7% to 84.1% for the ten malignant tumors. The mean and standard deviation of the WO volume fraction was 37.7 ± 18.5 (%) with the range from 11.1% to 74.2% for the 18 benign lesions, also significantly smaller than the value for the malignant tumors ($p < 0.002$). All three choices of using different postcontrast dynamic phases for the fitting produced similar results, demonstrating that the WO volume fraction analyis was not sensitive to these choices. (Among the three choices, the highest p-value of using the last three phases might reflect the least time points used in the fitting.) In comparison to the other two choices, using the last four phases for the fitting produced an optimal separation of the malignant tumors from the benign lesions and Fig. 9(B) shows a scatter plot of WO volume fraction versus lesion volume for the 28 suspicious breast lesions. The scattered distribution shows that the significant difference in the WO volume fraction between the malignant tumors and the benign lesions can be used to improve the characterization of suspicious contrast-enhancing breast lesions. If we choose 40% as a WO volume fraction threshold for characterizing these lesions [see the horizontal dashed-line in Fig. 9(B)], i.e., a WO volume fraction larger than the threshold would be characterized as malignant and a WO volume fraction smaller than the threshold would be characterized as benign, and then all of the ten malignant tumors would be characterized as malignant, maintaining the same sensitivity. However, 14 out of the 18 benign lesions would be characterized as benign, reducing the total number of the potentially unnecessary biopsies from 18 to 4 and consequently yielding a 77.8% reduction in the biopsy rate of benign lesions. Accordingly, this would result in an 100% improvement rate to the PPV of the biopsies (from 35.7% to 71.4%).

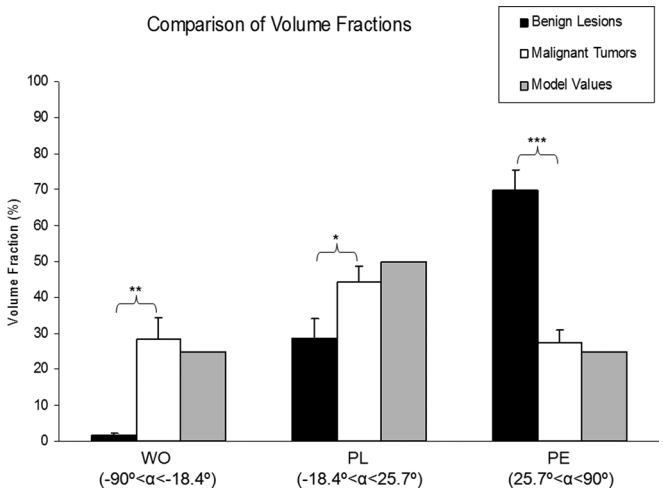

FIG. 7. Comparison of volume fractions of WO, PL, and PE between the benign lesions and the malignant tumors in study I for the cutoff boundary choice (1). The model values for the malignant tumors were computed using the Gaussian distribution in Fig. 3(A); the WO volume fraction (25%) is the area under the distribution for the range of $-90° < \alpha < -18.4°$, the PL volume fraction (50%) is the area for $-18.4° \leq \alpha \leq 25.7°$, and the PE volume fraction (25%) is the area for $25.7° < \alpha < 90°$. (*$p < 0.051$; **$p < 0.0012$; and ***$p < 0.0004$.) The error bar denotes SEM.

We also examined the effectiveness of using the lesion ROI-averaged signal intensity time course for improving the characterization of the 28 suspicious breast lesions. For each lesion at each time point, a lesion ROI-averaged signal intensity was computed by averaging signal intensity for all voxels within the lesion ROI, resulting in a mean signal intensity

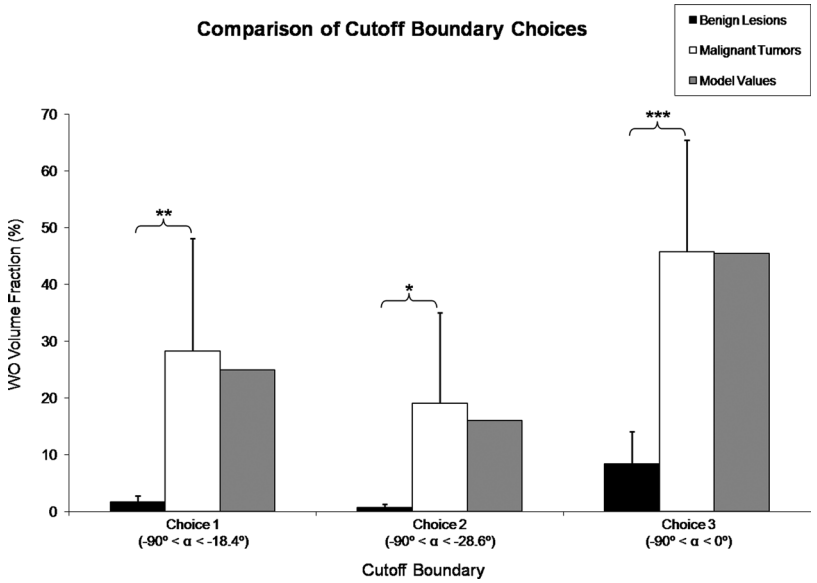

FIG. 8. Comparison of cutoff boundary choices for the differentiation of benignity from malignancy for the selected lesions in study I using WO volume fraction as a biomarker. The model values for the malignant tumors were computed for the three cutoff boundary choices using the Gaussian distribution in Fig. 3(A): for choice (1), the WO volume fraction (25%) is the area under the distribution for $-90° < \alpha < -18.4°$; for choice (2), the WO volume fraction (16%) is the area under the distribution for $-90° < \alpha < -28.6°$; and for choice (3), the WO volume fraction (45.6%) is the area under the distribution for $-90° < \alpha < 0°$. For each cutoff boundary choice, the mean WO volume fraction of the malignant tumors was in good agreement with the model-predicted value and was significantly larger than that of the benign lesions. (*$p < 0.004$; **$p < 0.002$; and ***$p < 0.001$.) Although the WO volume fraction values for both malignant and benign lesions varied from choice-to-choice, all three choices produced similar results, indicating the independence of the differentiation from the cutoff boundary choices. The error bar denotes σ.

time course for each lesion. Among the ten malignant tumors, two tumors showed WO behavior, four showed PL behavior, and the other four showed PE behavior. In contrast, among the 18 benign lesions, 15 lesions showed PE behavior, 2 showed PL behavior, and only 1 showed WO behavior. (Note that these descriptions were only qualitative.) The group-averaged mean signal intensity time course showed a PL curve for the malignant tumors but a PE curve for the benign lesions [Fig. 10(A)]. If we chose PE behavior for characterizing benign lesions, then the four malignant tumors with PE behavior would be incorrectly characterized as benign lesions.

Similarly, as we did previously for a voxel based approach, we also quantitatively examined the overall postcontrast kinetic behavior for a lesion using the lesion ROI-averaged signal intensity time course. A linear fitting of the mean signal intensity time course for the postcontrast five phases produced

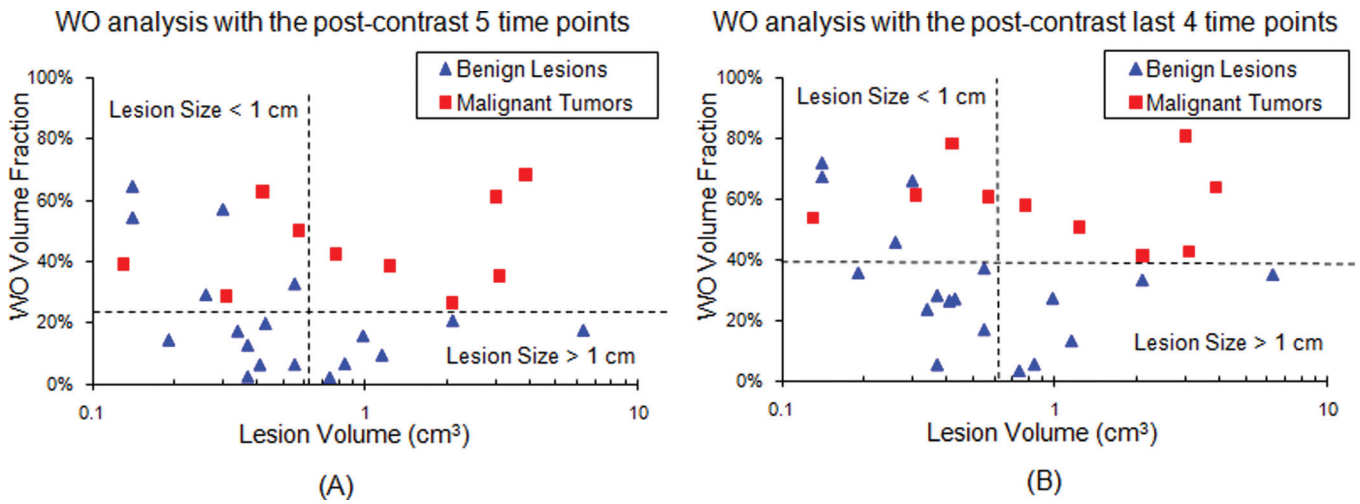

FIG. 9. Distribution of the WO volume fraction versus lesion volume for the malignant tumors and the benign lesions in study II with the voxelwise, least-squares linear fitting of the postcontrast signal intensity time course using (A) the whole five time points and (B) the last four time points. (B) The horizontal dashed-line indicates the 40% threshold value for characterizing these 28 suspicious lesions using the WO volume fraction as a biomarker: (1) all of the 10 malignant tumors would be characterized as malignant, maintaining the same sensitivity and (2) 14 out of the 18 benign lesions would be characterized as benign, reducing the total number of potentially unnecessary biopsies from 18 to 4. Note that the lesion size for the remaining four benign lesions is relatively small and the maximum one has an estimated lesion size of 8.3 mm with a sphere model. The vertical dashed-line separates the relatively small lesions (size < 1 cm) from the relatively large lesions (size > 1 cm).

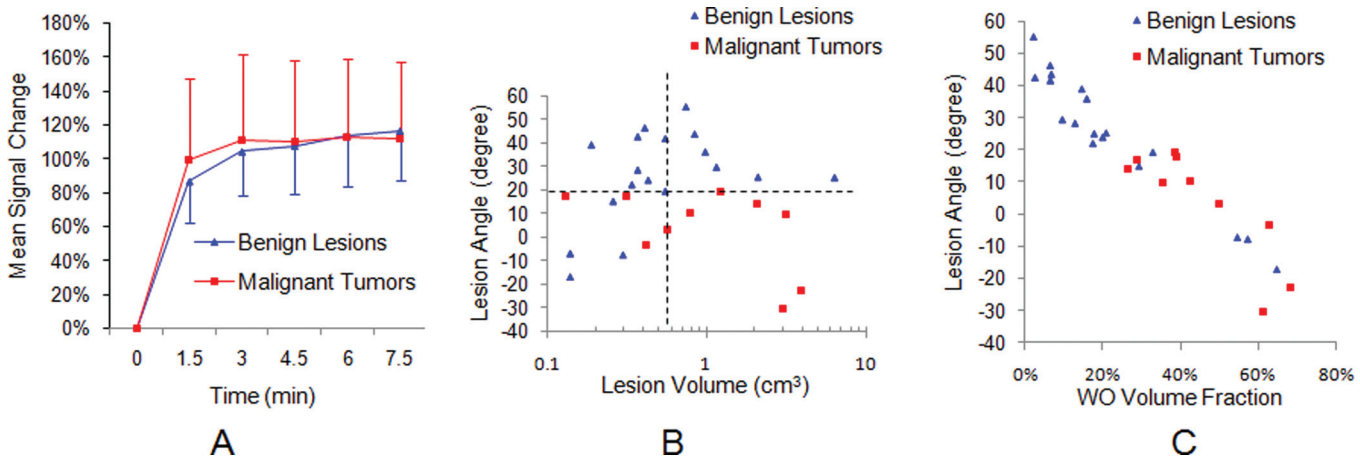

FIG. 10. Lesion ROI-averaged signal intensity time course analysis in study II. (A) The group-averaged mean signal intensity time courses for the benign lesions and the malignant tumors, respectively. The plotted signal change represents the postcontrast signal intensity change at each time point relative to the precontrast signal intensity. (B) Distribution of the lesion angle versus lesion volume for the 28 suspicious lesions. The horizontal dashed-line indicates the 20° threshold value for characterizing these lesions using the lesion angle as a measure, yielding the same results as using the measure of WO volume fraction in Fig. 9(A). (C) Association of the two measures (correlation coefficient $r = -0.95$, $P < 0.001$); when one measure went up, the other measure went down and vice versa.

a fitted straight line that depicted the overall postcontrast kinetic feature for the lesion. The corresponding slope and angle (lesion angle) of this fitted straight line were further computed using the same method described previously. For the ten malignant tumors, the mean and standard deviation of the lesion angle was 3.4° ± 17.4° with the range from −30.3° to 19.1°. For the 18 benign lesions, however, the mean and standard deviation of the lesion angle was 25.6° ± 19.8° with the range between −17.2° and 55.2°, significantly larger than the value for the malignant tumors ($p < 0.005$). This lesion angle provides another measure for improving the differentiation of the benign lesions from the malignant tumors, and Fig. 10(B) shows a scatter plot of lesion angle versus lesion volume for the 28 suspicious breast lesions. If we choose 20° as a lesion angle threshold for characterizing these lesions [see the horizontal dashed-line in Fig. 10(B)], i.e., a lesion angle smaller than the threshold would be characterized as malignant and a lesion angle larger than the threshold would be characterized as benign, and then all of the ten malignant tumors would be characterized as malignant, maintaining the same sensitivity. Interestingly, the same 13 benign lesions would be characterized as benign, yielding the same result of using the WO volume fraction as a measure [Fig. 9(A)]. The two measures were found to be strongly inversely correlated with each other (correlation coefficient $r = -0.95$, $P < 0.001$) [Fig. 10(C)].

IV. DISCUSSION AND CONCLUSIONS

Breast DCE-MRI has been shown to be very sensitive for breast malignant tumor detection. It is well recognized that, for optimal performance of dynamic MR imaging, it is crucial to evaluate the most enhancing (suspicious) areas of the lesion. The current standard ACR BI-RADS MR imaging lexicon recommends analyzing the enhancement rate and curve of a lesion by placing a manually selected ROI over the most intensely enhancing area of the lesion.[18] The curve shape is an important differentiator between malignant tumors and benign lesions for comparable enhancement rates and consequently the WO curve is an indicator for malignancy.[6,10] The kinetic WO curve was clearly present in each of the malignant tumors in both study I and study II. The WO curve, however, was also present in every one of the benign lesions in both studies, and was a major factor for their radiological characterization as suspicious lesions, resulting in the potentially unnecessary biopsies. In study II, although the sample size of 28 lesions is relatively small, the consequent 35.7% PPV of the biopsies of the sample reflects the current PPV of clinical practice at our site. The radiological diagnoses and subsequent biopsies of the 28 suspicious lesions were completely independent of this research study. In addition, this 35.7% PPV is consistent with the 33.6% PPV in a recent study which involved 125 suspicious lesions at another high volume breast MR clinical site.[17] In study II, the sample selection was unbiased, and the main purpose of the study is to test whether the WO volume fraction could be used as an additional MRI parameter for improving the characterization of suspicious contrast-enhancing breast lesions and consequently improving the PPV for biopsies in clinical breast MR practice.

To accurately measure the WO volume fraction of a lesion requires reliable lesion segmentation. Utilizing the difference in signal intensity of a contrast-enhanced lesion from its surrounding tissue, we tested a method for semi-automatically determining the lesion boundary in study I. The determined lesion boundary is objective and the subsequently computed WO volume fraction is also objective. The semi-automated method is a more time efficient method for measuring WO volume fraction compared to the manually drawn lesion. This semi-automatic method for lesion boundary determination and subsequently the automatic method for quantitative kinetic feature analysis and WO volume fraction computation should also improve the computer-based assessment in breast MRI, but a full test of possibly increased objectivity and efficiency to breast MR image interpretation is beyond the scope of this initial study.

For the suspicious lesions in study II, the WO volume fraction of the malignant tumors was found to be significantly larger than that of the benign lesions, supporting our hypothesis that the hypervascularity associated with tumor angiogenesis that is essential for cancer cell growth in malignant tumors produces a larger WO volume fraction for the malignant tumors. The significant difference in the WO volume fraction between the malignant tumors and the benign lesions could be used as an additional MRI parameter for improving the characterization of suspicious contrast-enhancing breast lesions [Fig. 9(B)]. If the WO volume fraction was used to characterize these suspicious lesions, the total number of potentially unnecessary biopsies could be reduced by 77.8% and the clinical 35.7% PPV of the biopsies would be improved to 71.4% PPV while maintaining the same sensitivity. If these results are confirmed in a large clinical trial, the WO volume fraction has the potential to improve the characterization of suspicious contrast-enhancing breast lesions in clinical practice, resulting in an improved PPV for biopsies and a subsequent reduction in the total number of benign biopsies.

The WO volume fraction may be a sensitive MRI parameter for characterizing suspicious contrast-enhancing breast lesions with a relatively large lesion size (>1 cm). There are a total of 12 large lesions (6 malignant tumors and 6 benign lesions) in study II (Fig. 9). For these large lesions, the distribution of the WO volume fraction for the malignant tumors was distinctly different from that for the benign lesions (Fig. 9), providing a measure to accurately differentiate these lesions. Accordingly, the WO volume fraction should have the potential to accurately differentiate benign versus malignant suspicious contrast-enhancing breast lesions in tumors greater than 1 cm if this study is later confirmed in a large clinical trial.

The WO volume fraction might also be helpful for improving the characterization of suspicious contrast-enhancing breast lesions with a relatively small size (<1 cm). There are a total of 16 small lesions (4 malignant tumors and 12 benign lesions) in study II [Fig. 9(B)]. For these small lesions, 8 out of the 12 benign lesions would be characterized as benign if the WO volume fraction was used for characterizing these small lesions, resulting in a 66.7% reduction rate in the total number of the 12 false-positive biopsies. The corresponding PPV of the biopsies of these small lesions would be improved from 25% to 50%. The remaining four false-positives, however, indicate that new or additional measures would be required to improve the characterization of small lesions.

It is worth pointing out that a reliable measure of lesion WO volume fraction requires a reliable segmentation of the lesion from its surrounding tissues. Our method is based on the postcontrast increased signal intensity of the lesion relative to the much less increased signal intensity of the surrounding tissues. Accordingly, the method is expected to be valid only for contrast-enhancing breast lesions.

It is also worth pointing out that the least-squares linear fitting of the postcontrast signal intensity time course mainly depicts the overall postcontrast kinetic behavior of the signal intensity time course. Considering that the computed value of angle α depends on the choice of time unit, in practical application it is desirable for the computed WO volume fraction to be independent of the unit choice. Unlike the other two cutoff boundary choices, the computed WO volume fraction value for the cutoff boundary choice (3) remains unchanged for different unit choices, yielding a desirable WO volume fraction measure. Although using the measure of lesion angle from the lesion ROI-averaged signal intensity time course analysis yielded the same results as that using the desirable WO volume fraction measure [Figs. 9(A) and 10(B)], the lesion angle threshold value varies with the choice of time unit which is a relative disadvantage when compared to the desirable WO volume fraction measure.

The main goal of this study was to introduce and test a new MRI measure of lesion WO volume fraction for improving the characterization of suspicious contrast-enhancing breast lesions. To the best of our knowledge, this measure has not yet been investigated. Our approach of lesion WO volume fraction analysis differs from those reported approaches in the literature that mainly rely on the ROI-based kinetic curve and kinetic feature analysis.[19–22] In a recent study Chen *et al.*[23] proposed a fuzzy c-means (FCM) clustering-based approach for automatically identifying characteristic kinetic curves of breast DCE-MRI images, classifying the signal intensity time courses of a segmented 3D breast lesion into a number of prototypic curves. The prototypic curve with the highest initial enhancement was selected as the representative characteristic kinetic curve of the lesion for further extracting the kinetic features that were used for testing the effectiveness of the differentiation between the benign and malignant lesions in comparison to other approaches. The study found that the classification performance of the proposed approach was similar to kinetic curves generated from regions drawn within the lesion by a radiologist experienced in breast MRI. If these drawn regions were the most highly enhancing (suspicious) areas of the lesion as recommended by the current standard ACR BI-RADS MR imaging lexicon in clinical practice, then the two approaches should yield a similar result because the prototypic curve with the highest initial enhancement was selected for the analysis. Chen *et al.*[23] also reported that the classification performance of their proposed approach was better than that from the curves obtained by averaging over the entire lesion. Our study found that although it is difficult to improve the differentiation of the benign lesions from the malignant tumors using the lesion ROI-averaged kinetic curves [Fig. 10(A)], the measure of lesion angles of these kinetic curves could improve the characterization of these suspicious lesions [Fig. 10(B)], reflecting its correlation with the measure of WO volume fraction [Fig. 10(C)].

In conclusion, we introduced and tested a novel MRI parameter of lesion WO volume fraction for improving the characterization of suspicious contrast-enhancing breast lesions. The study found that this new measure has the potential to nearly double the PPV of breast biopsies, avoiding 78% of the potentially unnecessary breast biopsies in clinical practice at our site. If these results are confirmed in a large clinical trial, then the new WO volume fraction

biomarker has the potential to improve computer-based assessment in breast MRI, and efforts should be made to incorporate this methodology in clinical computer-based software analysis programs.

ACKNOWLEDGMENTS

The authors thank Xuting Zou for processing image data for study II and appreciate Dr. E. J. Potchen and MSU Radiology for providing technical support. This work was supported in part by a Michigan State University IRGP New Directions grant. Tobias Hahn was supported by a graduate research assistantship from MSU Radiology. Partial results from these two studies were presented in recent ISMRM annual meetings.[24,25]

[a]Author to whom correspondence should be addressed. Electronic mail: jie@rad.msu.edu; Telephone: (517)884-3246; Fax: (517)432-2849.

[1]W. A. Kaiser and E. Zeitler, "MR imaging of the breast: Fast imaging sequences with and without Gd-DTPA," Radiology **170**, 681–686 (1989).
[2]S. H. Heywang, A. Wolf, E. Pruss, T. Hilbertz, W. Eiermann, and W. Permanetter, "MR imaging of the breast with Gd-DTPA: Use and limitations," Radiology **171**, 95–103 (1989).
[3]S. G. Orel, M. D. Schnall, V. A. LiVolsi, and R. H. Troupin, "Suspicious breast lesions: MR imaging with radiologic-pathologic correlation," Radiology **190**, 485–493 (1994).
[4]P. C. Stomper, S. Herman, D. L. Klippenstein, J. S. Winston, S. B. Edge, M. A. Arredondo, R. V. Mazurchuk, and L. E. Blumenson, "Suspect breast lesions: Findings at dynamic gadolinium-enhanced MR imaging correlated with mammographic and pathologic features," Radiology **197**, 387–395 (1995).
[5]F. Kelcz, G. E. Santyr, G. O. Cron, and S. J. Mongin, "Application of a quantitative model to differentiate benign from malignant breast lesions detected by dynamic, gadolinium-enhanced MRI," J. Magn. Reson. Imaging **6**, 743–752 (1996).
[6]C. K. Kuhl, P. Mielcareck, S. Klaschik, C. Leutner, E. Wardelmann, and J. Gieseke, H. H. Schild, "Dynamic breast MR imaging: Are signal intensity time course data useful for differential diagnosis of enhancing lesions?" Radiology **211**, 101–110 (1999).
[7]S. G. Orel, "Differentiating benign from malignant enhancing lesions identified at MR imaging of the breast: Are time-signal intensity curves an accurate predictor?" Radiology **211**, 5–7 (1999).
[8]K. Kinkel, T. H. Helbich, L. J. Esserman, J. Barclay, E. H. Schwerin, E. A. Sickles, and N. M. Hylton, "Dynamic high-spatial-resolution MR imaging of suspicious breast lesions: Diagnostic criteria and interobserver variability," Am. J. Roentgenol. **175**, 35–43 (2000).
[9]D. A. Bluemke, C. A. Gatsonis, M. H. Chen, G. A. DeAngelis, N. DeBruhl, S. Harms, S. H. Heywant-Kobrunner, N. Hylton, C. K. Kuhl, C. Lehman, E. D. Pisano, P. Causer, S. J. Schnitt, S. F. Smazal, C. B. Stelling, P. T. Weatherall, and M. D. Schnall, "Magnetic resonance imaging of the breast prior to biopsy," JAMA **292**, 2735–2742 (2004).
[10]M. D. Schnall, J. Blume, D. A. Bluemke, G. A. DeAngelis, N. DeBruhl, S. Harms, S. H. Heywant-Kobrunner, N. Hylton, C. K. Kuhl, E. D. Pisano, P. Causer, S. J. Schnitt, D. Thickman, C. B. Stelling, P. T. Weatherall, C. Lehman, and C. A. Gatsonis, "Diagnostic architectural and dynamic features at breast MR imaging: Multicenter study," Radiology **238**, 42–53 (2006).
[11]C. Frouge, J. M. Guinebretiere, G. Contesso, R. D. Paola, and M. Blery, "Correlation between contrast enhancement in dynamic magnetic resonance imaging of the breast and tumor angiogenesis," Invest. Radiol. **29**, 1043–1049 (1994).
[12]L. D. Buadu, J. Murakami, S. Murayama, N. Hashiguchi, S. Sakai, K. Masuda, S. Toyoshima, S. Kuroki, and S. Ohno, "Breast lesions: Correlation of contrast medium enhancement patterns on MR images with histopathologic findings and tumor angiogenesis," Radiology **200**, 639–649 (1996).
[13]D. L. Buckley, P. J. Drew, S. Mussurakis, J. R. T. Monson, and A. Horsman, "Microvessel density of invasive breast cancer assessed by dynamic Gd-DTPA enhanced MRI," J. Magn. Reson. Imaging **7**, 461–464 (1997).
[14]M. Y. Su, Y. C. Cheung, J. P. Fruehauf, H. Yu, O. Nalcioglu, E. Mechetner, A. Kyshtoobayeva, S. C. Chen, S. Hsueh, C. E. McLaren, and Y. L. Wan, "Correlation of dynamic contrast enhancement MRI parameters with microvessel density and VEGF for assessment of angiogenesis in breast cancer," J. Magn. Reson. Imaging **18**, 467–477 (2003).
[15]E. S. Fobben, C. Z. Rubin, L. Kalisher, A. G. Dembner, M. H. Seltzer, and E. J. Santoro, "Breast MR imaging with commercially available techniques: radiologic-pathologic correlation," Radiology **196**, 143–152 (1995).
[16]A. Iglesias, M. Arias, P. Santiago, M. Rodriguez, J. Manas, and C. Saborido, "Benign breast lesions that simulate malignancy: Magnetic resonance imaging with radiologic-pathologic correlation," Curr. Probl. Diagn. Radiol. **36**, 66–82 (2007).
[17]L. C. Wang, W. B. DeMartini, S. C. Partridge, S. Peacock, and C. D. Lehman, "MRI-detected suspicious breast lesions: Predictive values of kinetic features measured by computer-aided evaluation," Am. J. Roentgenol. **193**, 826–831 (2009).
[18]E. A. Morris, "Breast MR imaging lexicon updated," Magn Reson Imaging Clin N Am **14**, 293–303 (2006).
[19]S. Mussurakis, D. L. Buckley, and A. Horsman, "Dynamic MRI of invasive breast cancer: Assessment of three region-of-interest analysis methods," J. Comput. Assist. Tomogr. **21**, 431–438 (1997).
[20]G. P. Liney, P. Gibbs, C. Hayes, M. O. Leach, and L. W. Turnbull, "Dynamic contrast-enhanced MRI in the differentiation of breast tumors: User-defined versus semiautomated region-of-interest analysis," J. Magn. Reson. Imaging **10**, 945–949 (1999).
[21]T. Niemeyer, C. Wood, K. Stegbauer, and J. Smith, "Comparison of automatic time curve selection methods for breast MR CAD," Proc. SPIE, **5370**, 785–790 (2004).
[22]W. Chen, M. L. Giger, L. Lan, and U. Bick, "Computerized interpretation of breast MRI: Investigation of enhancement-variance dynamics," Med. Phys. **31**, 1076–1082 (2004).
[23]W. Chen, M. L. Giger, L. Lan, U. Bick, and G. M. Newstead, "Automatic identification and classification of characteristic kinetic curves of breast lesions on DCE-MRI," Med. Phys. **33**, 2878–2887 (2006).
[24]J. Huang, T. Hahn, L. Hoisington, and K. Berger, "Accurately differentiating benign from malignant contrast-enhancing breast lesions using an automated method of quantitative washout kinetics and fractional lesion volume analysis," Proc. Int. Soc. Magn. Reson. Med. **17**, 4245 (2009).
[25]J. Huang, L. Hoisington, S. Schafer, X. Zong, and K. Berger, "Improving suspicious breast lesion characterization using lesion fractional volume washout kinetic analysis," Proc. Int. Soc. Mag. Reson. Med. **18**, 2799 (2010).